Hemodynamic Simulations to Identify Irregularities in Coronary Artery Models

K. E. Hoque[1*], S. Sawall[2], M. A. Hoque[1] and M. S. Hossain[1]

[1]*Department of Arts and Sciences, Ahsanullah University of Science and Technology, Dhaka-1208, Bangladesh.*

[2]*X-Rays and CT-imaging, German Cancer Research Center (DKFZ), Heidelberg, Germany.*

Authors' contributions

Article Information

Original Research Article

Abstract

Objectives: Nowadays invasive coronary angiogram is a gold standard clinical application to determine fractional flow reserve (FFR) over the world. The engineering tools computational fluid dynamics (CFD) enabled the simulation of coronary blood flow conditions in the idealized and patient-based coronary models. The CTA-based CFD simulation allowed us to produce a non-invasive assessment of the hemodynamic parameters, such as blood velocity magnitude, relative pressure difference and virtual fractional flow reserve (vFFR). These hemodynamic mechanisms provide the information on coronary stenosis conditions and predict the severity of coronary arterial lumen area which is responsible for the heart attack of the human patients.

*Corresponding author: E-mail: ekram_math.as@aust.edu

Methodology: In the current study investigates the hemodynamic parameters by using idealized coronary artery prototypical model and patient-specific real coronary artery models. The patient-specific model reconstructed by following steps: CTA image acquisition, image segmentation, 3D reconstruction, smooth surface and computational mesh generation. The hemodynamics simulation derived by solving the Navier-Stokes equations for steady and pulsatile flow motions.

Results: The results reflect expected outcomes in both cases, for instance, a higher blood velocity in the coronary vessels tends to stretch the contrast agent gradient and a lower blood velocity magnitude tends to steepen the contrast agent gradient. The pressure difference and vFFR results allow to distinguish the unstenosed and stenosis arterial models.

Conclusion: The aim of the work was to set up a framework for an idealized and a patient-specific models reconstruction, geometric analysis and describing hemodynamic parameters. The parameters allowed to describe the intrinsic blood flow in a non-invasive procedure. The simulation results are feasible for clinical applications but there are some limitations in the approaches which need more studies to overcome them.

1 Introduction

The interruption of blood flow in crucial organs like the heart and brain can lead to death which is known as cardiovascular disease. The cardiovascular abnormalities especially, coronary artery diseases are the leading cause of death in modern society. In 2010, 29.6% of total deaths of worldwide were caused by cardiovascular diseases [1]. According to the World Health Organization (WHO), 17.5 million people died from cardiovascular diseases in 2012, representing 31% of all global death while 7.4 million due to coronary heart diseases and 6.7 million due to stroke. There are different cardiovascular diseases but atherosclerosis and arteriosclerosis are the two most common of them. Atherosclerosis is a chronic and cumulative complex disease that typically starts in the early childhood and progresses slowly as people grow older [2]. A number of risk factors has been associated with atherosclerosis, such as genetic predisposition, hypertension, smoking, hyperlipidemia, viral infection, social stress and a sedentary lifestyle. The advanced medical imaging technique, for instance, coronary computed tomography angiography (CTA) had emerged as a non-invasive procedure for direct visualization of the atherosclerotic disease [3], [4]. The combination of CFD and CTA technologies enables a simulation of coronary blood flow conditions in a patient-based coronary model that allows the non-invasive assessment of ex-vivo hemodynamic parameters including blood velocity, pressure difference, vFFR [5], [6]. These diagnostic procedures could serve as a gatekeeper for unnecessary and conventional invasive catheterization and vFFR outcomes may be suggested for the surgical procedure of coronary revascularization [7]. The stenosis of the coronary arteries is usually caused by atherosclerosis where the hemodynamic significance of patient-specific coronary stenoses and the risk assessed by comparing the hemodynamic effects induced by blood flow motions [8]. The CFD with CTA technique is not only saving direct healthcare costs but also will reduce indirect costs and patient risks, such as heart attack, stroke and death [9]. In this study, there are two models for hemodynamic simulation such as 3D coronary ideal model and CTA based patient model. In the ideal case, the idealized models were generated by using computer-aided design software and the patient-based models from computed tomography angiography (CTA) imaging data. We applied manually different sizes of atherosclerotic stenoses which took place near bifurcations or bending regions in the computational domains. The arterial bifurcation regions are very vulnerable for the progression of atherosclerosis disease [10]. The computer-aided design

open source software generates the 3D ideal model and patient-based model generated from CTA imaging data. The imaging data collected from a non-invasive procedure does not violate the ethical principle of The World Medical Association Declaration of Helsinki. The ideal model imitates the structure of real coronary artery and the patient-based right main coronary artery extracted from the CTA images which produced after proper segmentation and three-dimensional reconstruction. The coronary CTA provides high sensitivity i.e. high negative predictive value where anatomical information is available [11]. Nowadays, the iterative 3D image reconstruction along with multidetector CT and ECG-gated allows the CTA scanning with morphological details of coronary vessels [12]. But CTA itself does not provide any physiological or functional assessment of lesion severity in coronary artery [13], [14] and [15]. Unlike coronary blood flow simulation, CFD studies on intra-cardiac flows are primarily confined to research purposes owing to the complexity of modeling intra-cardiac flows that emerge as new cardiac diagnostics and therapeutics of the heart has given the virtual design and testing of technologies in a patient-specific environment [16].

In this study, we have applied several techniques for patient-based model simulation, such as the CTA image segmentation, 3D reconstruction, smooth surface generation and the shrink wrapping grids generation in the models. The application procedure of the hemodynamics technique has been used by some important mathematical tools for the 3D idealized model and patient-based model. Then we have assigned some unavoidable mathematical formulae which solve in the discretization nodes of the computational models that hass been discussed in the next sections.

2 Mathematical Formulation

2.1 Governing equations

The application procedure of the hemodynamics technique has been used by some important mathematical tools for the 3D idealized model and patient-based models. We considered two type of flows for numerical simulations, one was steady and another one was pulsatile flow. The hemodynamics simulation derived by solving the Navier-Stokes equations without gravitational constant where blood considered as an incompressible fluid which can be represented by the equations:

$$\rho\frac{\partial \mathbf{u}}{\partial t} + \rho(\mathbf{u}\cdot\nabla)\mathbf{u} + \nabla P = \mu\nabla^2\mathbf{u}, \qquad \nabla\cdot\mathbf{u} = 0, \tag{2.1}$$

where $\mathbf{u}$ is the blood flow velocity, P is the pressure, ρ and μ are the density and dynamic viscosity of the blood respectively. In the prototypical coronary and real patient models, the blood flow follows the Stokes relation

$$\tau = \mu[\nabla\mathbf{u} + (\nabla\mathbf{u})^T] + (\frac{2}{3}\mu - \kappa)(\nabla\cdot\mathbf{u})I, \tag{2.2}$$

where $\nabla\mathbf{u}$ is the velocity gradient vector, I is the identity vector and κ is the dilatational viscosity. For incompressible fluid, the equation (2.2) becomes,

$$\tau = \mu[\nabla\mathbf{u} + (\nabla\mathbf{u})^T].$$

Blood velocity, in the computational domains, was the constant of the ratio of the shear stress and shear rate. In the idealized model, we applied laminar flow with a Reynolds number of 183, where the flow velocity is $\mathbf{u} = 16.1 \ cm/s$. For the pressure variation of steady and pulsatile blood flow simulation was represented by the equation

$$\Delta P = P_{steady} + P_{pulsatile}\sin(2\pi.K.t), \tag{2.3}$$

where $K = HR/60 = 1$, HR= 60bpm, is the heartbeats per minute and P_{steady} is steady flow pressure that is considered as 3 mmHg and $P_{pulsatile} = 2.75$ mmHg. The above sinusoid equation imitated the pulsatile flow pattern but did not reflected the exact physiological phenomenon of the human arterial blood flow condition. For the boundary of the computational models, we employed the no-slip condition for the vessel walls. The another boundary condition is known as Neumann type of boundary condition that we selected for inlet and outlet/s in computational domains. The governing equation given below indicates the transport of the blood contrast agent concentration.

$$\frac{\partial C}{\partial t} + (\mathbf{u} \cdot \nabla)C = D\nabla^2 C, \tag{2.4}$$

where C is the contrast agent, $D = \frac{\mu}{\rho} \cdot \frac{1}{Sc}$ is the molecular diffusivity of the blood contrast agent and $\mathbf{u}$ is the flow velocity obtained from Navier-Stokes equations and Sc is known as Schmidt number. The governing equation provided the value of the contrast agent concentration. In reality, it is suitable to give an arterial input function for contrast agent dispersion that mimics the blood flow behavior in the computational arterial models.

2.2 Analytic approach and velocity profile validation

For validation of computational results, we established a comparative study of the computational simulation and analytical approach for a velocity profile. The analytic solution of a laminar and incompressible fluid flow demonstrated in the computational velocity profile in a pipe flow. The velocity profile in terms of r (radius of the inside profile) represents the second order differential equation

$$\frac{d^2\mathbf{u}}{dr^2} + \frac{1}{r}\frac{d\mathbf{u}}{dr} = -\frac{1}{\mu}\frac{dP}{dr}. \tag{2.5}$$

This is the general equation for a steady, laminar, incompressible pipe flow in the fully developed region. The general solution of the above ordinary differential equation (2.5), we considered

$$\mathbf{u}(r) = A + Br^2, \tag{2.6}$$

where A and B are the constants which must be fit to the no slip boundary conditions where the blood velocity is $\mathbf{u} = 0$ at $r = R$ along the vessel walls. The solution of the differential equation (2.5) is

$$\mathbf{u}(r) = \frac{1}{4\mu}\frac{\Delta P}{\Delta x}(R^2 - r^2). \tag{2.7}$$

Where the equation (2.7) is the velocity profile equation and μ is the dynamic viscosity of blood, R is the radius of the blood vessel, Δx is the length of the vessel (Fig:1(a)) and ΔP is the relative pressure difference of the vessel area. In the Fig. 1, it is distinct that the laminar flow velocity profile growing from the outset position of the vessel by following after a certain time [17]. The profile is fully developed and gives a parabolic shape which is generated by finite element method (FEM) simulation software (see appendix). For a computational and analytic purpose, we chose a vessel with radius 2 mm and inlet velocity 16.3 cm/s. The Fig: 1(b) shows that the analytic solution and FEM simulation result in assigned almost similar value which is 24.3 cm/s for the inlet velocity 16.3 cm/s. The coincidence results help the current study to understand the fully developed laminar velocity profile numerically rational.

3 Idealized Model

In general, an idealized coronary artery model is a prototypical model that mimics an original patient-specific coronary artery model. An idealized model gives some ideas that are easy to understand compared to a realistic patient model. Blood flow in the cardiovascular circulation,
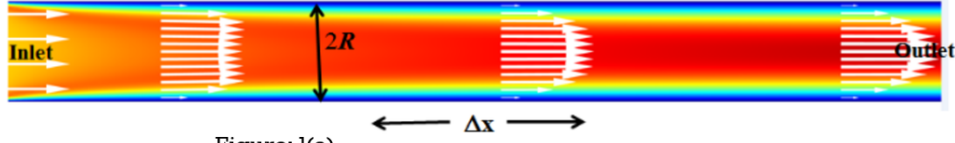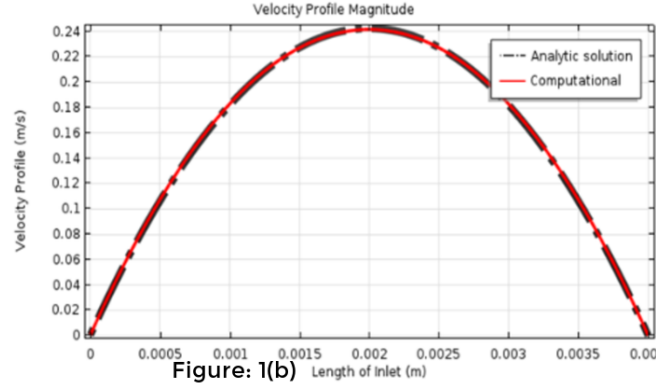
Figure: 1(a)

Figure: 1(b)

Fig. 1. The computational result (Figure:1(a)) and analytical result (equation (2.7)) represent graphically (Figure: 1(b)) where both results for the fully developed laminar velocity profile coincide each other. The computational result (Fig :1(a)) and analytical result (equation (2.7)) represent graphically (Figure: 1(b)) where both results for the fully developed laminar velocity profile coincide each other.

especially in the coronary arteries circulation is quite complex to comprehend in an experimental way. If we employ all physical materials and set up a framework properly with all requirements then an ideal model gives a general concept of the exact result of the intricate blood circulatory system. In this section, we present a study of an idealized healthy, one stenosis and two stenoses models for steady and pulsatile blood flow simulation. in the next section, we will apply the same strategies for patient-specific model simulation.

3.1 Construct of idealized 3D models

Constructing a computational idealized model remains a challenging procedure by following all criteria of an original patient-based model. From the anatomical view, it is quite clear that the most of the coronary main arteries are bifurcated everywhere. In general, most of the stenosis occur near the bifurcations or artery bending regions. For supporting these characteristics, we generated a 3D model consisting of one main vessel and its two branches. The length of the main artery is approximately 15 *cm* where the proximal radius is 2 *mm* and distal radius is 1.4 *mm* by following the clinical data [18]. The position of the first branch artery is located 4 *cm* from ostium and the second branch is assembled 6 *cm* distance from the distal area of the main vessel. The length and radius of the proximal branch are 10 *cm* and 1.7 *mm* respectively. The length and radius of the distal branch prototypical artery are 6 *cm* and 1.1 *mm* respectively. For curving the model a B-spline function is a good option that is easy to handle for bending the main and branch arteries. For building the arterial inside and outside of the wall, we built two times 3D model around the same B-spline, where the position and orientation are same but radius is different. The different radii make the thickness of the idealized coronary artery model. By applying boolean function we got a nice shape of the 3D model. The stenosis (diseased) of the idealized model was generated manually

5
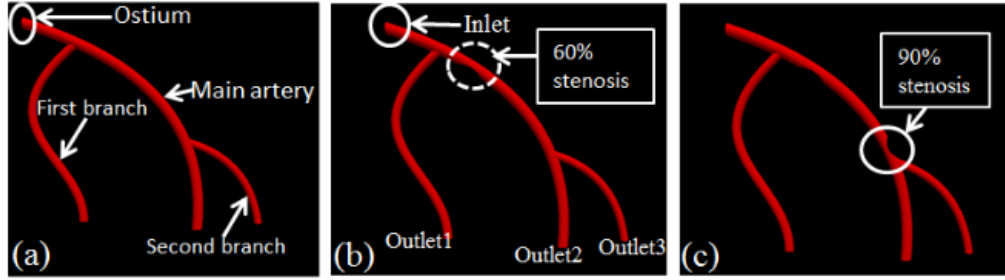
Fig. 2. 3D idealized model of the coronary artery, (a) the normal (unstenosed) model with two bifurcations and the ostium represents the root of artery from aorta, (b) one stenosis artery model with around 60% severity, (c) in two stenoses artery model, the second stenosis area reduced manually approximately 90% in a severe case.

on the main vessel. The two stenoses were built up under and above the surface of the model from the view position and these are located in between the two bifurcations. The first stenosis is located just after the first branch of artery where the severity (area reduction) is approximately 60% and the second stenosis is located just before second branch of artery with the severity around 90% of the main artery (Fig. 2). Therefore, this computational model contains one inlet and three outlets that are represented by outlet1, outlet2 and outlet3 in the Fig. 2(b). The structure and dimension of the model are based generally on a typical left coronary artery that follows the anatomically close information. For FEM simulation, it is better to save the model in STEP file format that produces smooth boundary walls with inlet and outlets in the ideal domains.

3.2 Grid generation in 3D idealized model

The first and foremost stage of the numerical simulation is the proper grid or mesh generation in the 3D computational domain. The idealized model generated by computer-aided design (CAD) software. Then the 3D model was exported in a suitable file format from the CAD software which produced the 3D model with a uniform shape. Finite element mesh generation provided a concise and comprehensive mesh solution over curved surfaces and 3D volume cells. After importing the .step file in the FEM simulation software, assigned the surface and boundary areas discretization by the unstructured adaptive triangular cells and tetrahedral cells. The finer unstructured cells provided a smooth shape on the surface and boundaries of the computational 3D models. In the same way, in the fluid zone (an internal volume of boundaries) covered by unstructured tetrahedral cells where the maximum cell size was 1 mm and the minimum cell size was 0.7 mm. A finer unstructured meshing gives high-quality mesh that improves numerical stability and increases the likelihood of attaining a reliable solution [19]. In the whole domain, the amount of mesh was 1.07718×10^5 elements, where 86164 in the fluid zone, 20322 in boundary elements and 1432 in edge elements. The other parameters for the meshing of the growth rate was 1.5, the curvature factor was 0.6 and resolution in narrow regions was 0.5. In Fig. 3, the unstructured mesh pattern over the surface especially in the bifurcation area is more distinct. After completing computational mesh generation in the 3D model that needs to integrate with the hemodynamical mathematical discrete equations for the solution of biofluid simulation are discussed in the next section.
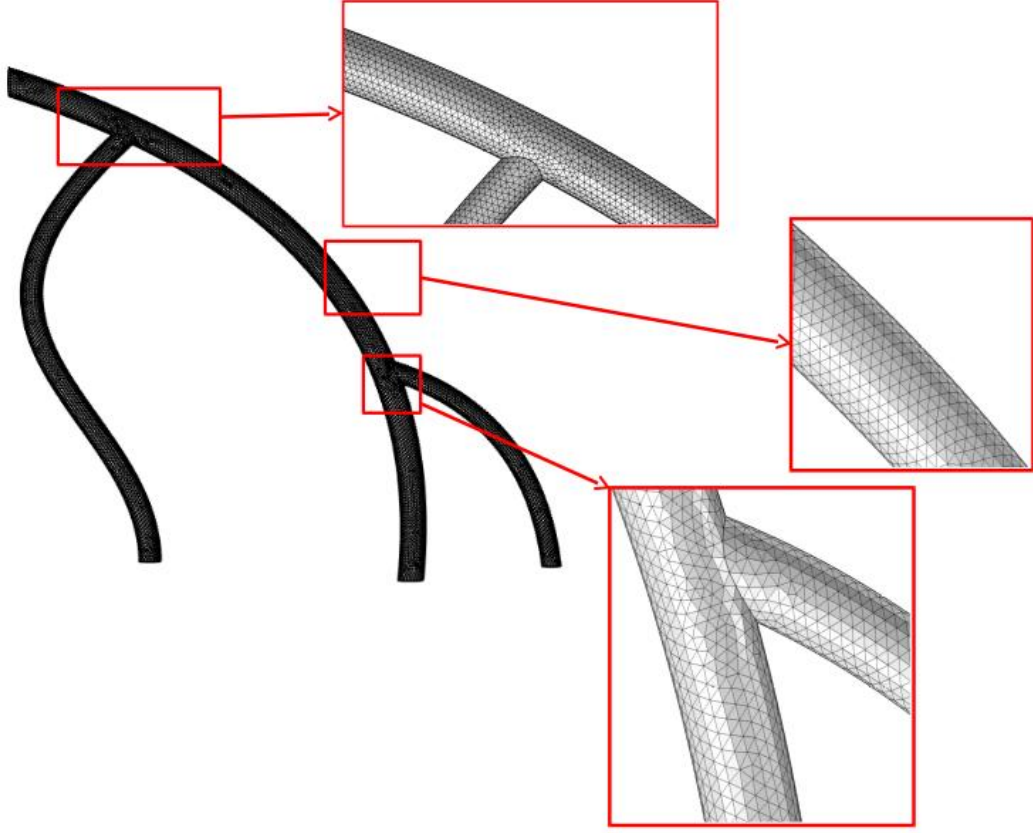
Fig. 3. Computational grids generated in the different segments of the idealized 3D model.

## 3.3 Arterial input function and comparison of simulation results

The arterial input function (AIF) plays an important role to measure the blood contrast agent concentration under the time-dependent condition at the outset position of the coronary artery. AIF immitated the multislice CT scans image which employed for automatic bolus tracking in the reference position at ostium where image acquisition started at some assigned HU (Hounsfield units) in Fig. 4. The attenuation coefficient in HU is directly proportional to the contrast agent concentration [20]. The following AIF that described in [21] is defined as

$$C(t) = C_{\min} + 0.5 \cdot S_{ostium}(C_{\max} - C_{\min}), \tag{3.1}$$

where $C_{\max}$ and $C_{\min}$ represent that the CTA image acquisition CT values.

$$S_{ostium} = (1 - \cos\frac{\pi(t - t_s)}{T_d}),$$

here T_d is the time-delay between the bolus arrival and maximum enhancement in Fig. 4 and t_s is the starting position of the bolus. In the case, we consider the typical values of $C_{\max} = 350$ HU, $C_{\min} = 50$ HU, $T_d = 15$ s, and $t_s = 10$ s for performing AIF. Fig. 4 shows a smooth rise from a minimum value 50 HU to the maximum contrast agent enhancement value of 350 HU. The
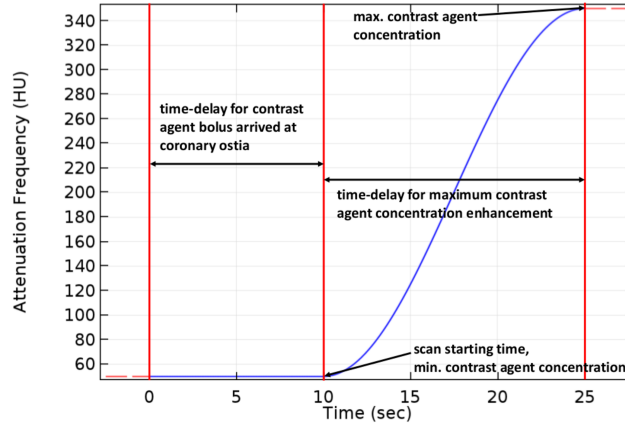
Fig. 4. The AIF generates the contrast agent concentration for biofluid simulation in the computational domains.

numerical simulation was performed for the steady and pulsatile flows with the area of stenosis around 60% and 90%. The computational results provided the elative pressure difference and velocity magnitude for the idealized model coronary artery. In the steady case, the density of blood 1060 kg/m^3 and laminar flow with the Reynolds number 183. The Lamé parameters handle the artificial tube stress and strain of the arterial elasticity. The inlet and outlets values of the idealized model followed by the Neumann type boundary condition and selected the no-slip condition for boundary walls. The inlet velocity value allocated 16.1 cm/s and outlets allocated pressure around 3 $mmHg$. For comparing, the simulation results with the clinical study, we built two tables below for steady and pulsatile flows.

Data comparison for steady flow:

Table 1: The table represents our simulation results in idealized model for steady flow with various severity of stenosis, all values represent the biofluid velocity magnitude in cm/s.

	Normal	One stenosis	Two stenoses
Inlet	17.1	20	19.7
Outlet2	11	10	6.2
Disease area		33.33	14 and 18.2
First branch	11	19	23
Second branch	7.5	6	5

Data comparison for pulsatile flow:

A clinical study on coronary arterial average blood velocity [22] in the left anterior descending (LAD) coronary artery refers 17.98 ± 5.66 cm/s that was measured by using digital tracking technique. For the pulsatile flow simulation case, the similar strategies followed for physical materials, boundary

Table 2: The table shows our simulation results of idealized model for pulsatile flow with different severity of stenosis, all values represent the biofluid velocity magnitude in *cm/s***.**

	Unstenosed	One stenosis	Two stenoses
Inlet	20	24	21.3
Outlet2	15.5	14.2	6.1
Disease area		57.8	32.7 and 44
First branch	12	19	19.4
Second branch	14.5	13.4	10

conditions and mesh generation where the sinusoidal function imitates the pulsatile flow behavior. This is obvious that the outputs are physically feasible and lay between the upper and lower limit of the published literature.

3.4 Visualization of simulation results in coronary ideal models

The postprocessing is one of the most important stages for numerical simulation of coronary arterial blood flow. The CFD solver (see Appendix) produced the simulation results, after set-up of all physical materials and different boundary conditions properly.

The Fig. 5. has two rows, where the first row represents the velocity magnitude of the different conditions (unstenosed, one and two stenoses). The unstenosed model simulation shows the uniform velocity over the entire main tube and less velocity in the branch tubes (see table results).

The second image **(b)** of the same figure indicates that the upstream and downstream velocity difference are more obvious blood flow in the stenosis area. Due to the stenosis in the main vessel, the flow of blood was much higher in the stenosis region than other locations. In the two stenoses model, the blood flow displayed highest velocity in the second stenosis region which was more clear. These characteristics of the stenosis models represented the physiological phenomena in the steady flow state. The relative pressure also illustrated the physically viable conditions, such as in the unstenosed model, the relative pressure in different locations of the model was uniform. The one stenosis or two stenoses model refered the relative pressure differences were very distinguishable between the upstream and downstream of lesion areas. In the steady blood flow simulation, we measured the vFFR value which showed the physiological phenomenon of the stenosis condition.

In the one stenosis model simulation results illustrated that the upstream relative pressure was 4.05 *mmHg* and the downstream relative pressure was 3.23 *mmHg* of the first stenosis region. The vFFR value gave from the ratio of the downstream and upstream relative pressure of the stenosis model was ≈ 0.80 which represented the stenosis was not very sever [23]. The second stenosis was more significant as expected where the vFFR value ≈ 0.51.

The pulsatile flow simulation was similar with the results of the steady flow as expected. For the visualization of the computational results in Fig. 6, assigned the same scale in velocity magnitude. It can be distinguishable in visual ways that flow velocity patterns differ from one another. The velocity segment with flow vectors were magnified separately which provided the inside of the blood flow condition. The relative pressure difference results were very similar to steady flow. The vFFR value around the same values which produced in two stenosed arteries. In this study, the blood flow simulation in different physiological conditions gave feasible results in the 3D idealized model.
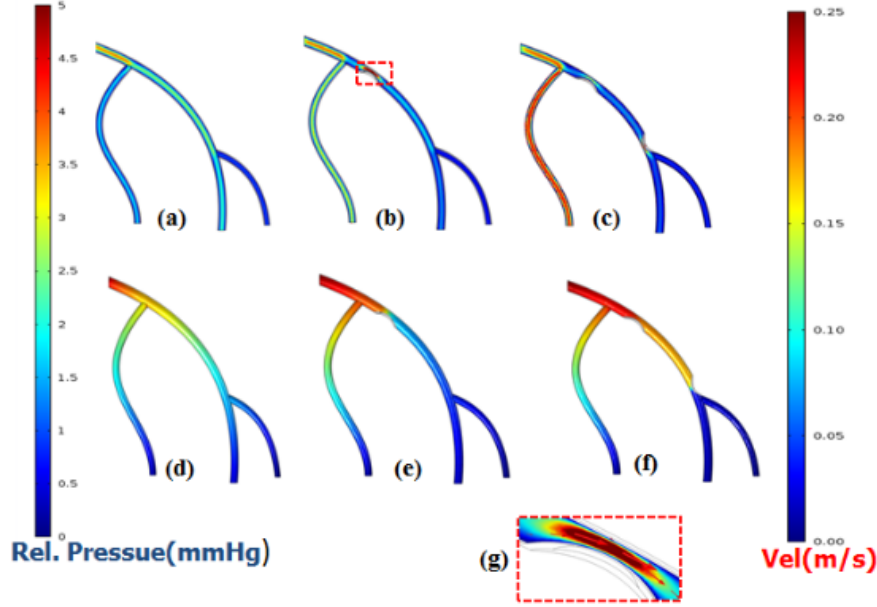
Fig. 5. The steady flow simulations in the idealized 3D model represent in (a) unstenosed model velocity magnitude, (b) one stenosis about 60% lesion velocity flow and the segment of the lesion area with velocity vectors represent separately in (g), which measures the orientation of blood flow pattern, (c) two stenoses model simulation where the second stenosis indicates the severe case and in the second row, the images (d), (e), (f) represent the relative pressure of (a), (b), (c) model respectively.

4 Patient-based model

The blood flow simulation of the patient-based coronary model was more challenging than the ideal model. The same strategies followed for the patient-specific model which allocated for the idealized model in hemodynamic simulation. The 3D patient model reconstruction was executed with a few steps, such as CTA image acquisition, image segmentation, 3D reconstruction, smooth surface and computational mesh generation.

4.1 Cardiac CT image acquisition

CT is a nondestructive 3D imaging technique for visualizing interior features within the patient's body and forming digital information for 3D image reconstruction. The cardiac CT image acquisition follows the same principle as normal CT scan procedure except contrast dye injection. The multislice (64-slice or 320-slice) scanner provides highly detailed temporal resolution of the coronary artery CT scans [24].

The CTA data (the CTA data collected from X-Ray Imaging and Computed Tomography, German Cancer Research Center, Heidelberg, Germany) with volume $512 \times 512 \times 376$, where each slice size was 512×512 and depth was 376. The slice position 115 among the 376 slices displayed in Fig. 7 that provided visual information about the anatomical detailed, such as the aorta, right and left
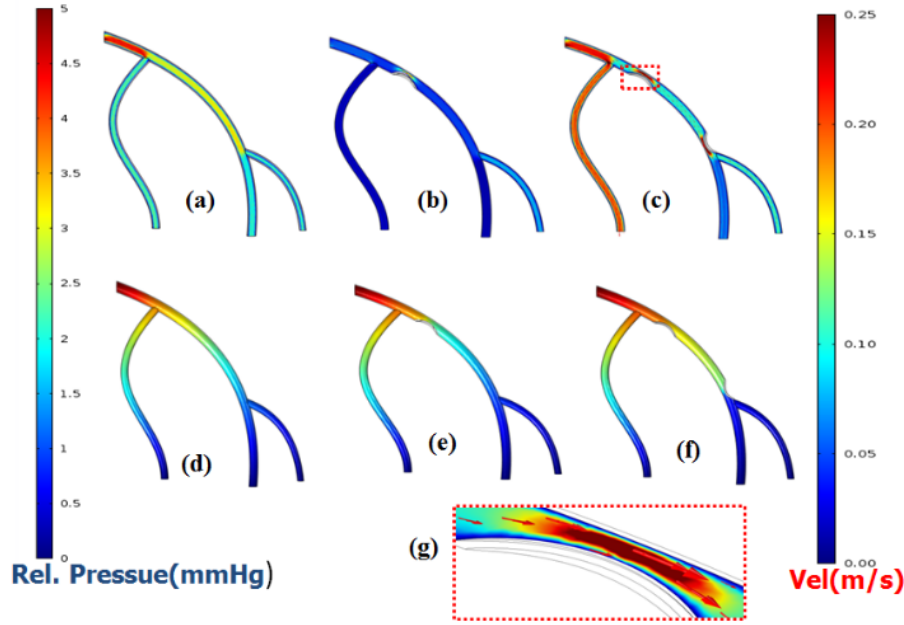
Fig. 6. The pulsatile flow simulation in the idealized 3D model represent (a) unstenosed, (b) one stenosis and (c) two stenoses model velocity magnitude and the second stenosis indicates the sever case and the segment of the lesion area with velocity vectors represent separately in (g), the second row, the images (d), (e), (f) represent the relative pressure of the corresponding images (a), (b), (c), respectively.

coronary arteries. The radius of the coronary arteries was 2.5 mm. The resolution of the CT image was high and the voxel spacing was $(0.39, 0.39, 0.3)$. The computational simulation was performed in the right main coronary artery (RCA) by using this raw data.

4.2 Image segmentation and 3D reconstruction from 3D patient data

The CTA image segmentation and 3D reconstruction were two of the challenging steps for CHD simulation. The CTA data was segmented by a threshold-based method (see Fig.7). The thresholding segmentation algorithm was allowed to segment the 32 bit real cardiac CT images to binary (black refers the pixel value is 0 and white that the pixel value is 1) image by applying histogram analysis technique. The histogram tool captured the target area from CT scans of the coronary arteries. The binary image produced a significant view of RCA which was connected with the largest artery aorta. The connecting region extraction algorithm combined with cutting section technique allowed us to separate the RCA from the aorta and eventually from the entire CTA data. The consequent reconstruction procedures of a 3D model were performed by using an open source software described in the Appendix. At last, the 3D model was exported by using computer-aided file format .stl from the segmentation software. In the next step, the computational domain was reconstructed by the smooth surface, because the exported model was not allowed in CFD solver for simulation due to the model complication such as some grids intersected each other. For suitable surface reconstruction on the 3D segmented model, the marching cubes algorithm a good alternative for smooth mesh
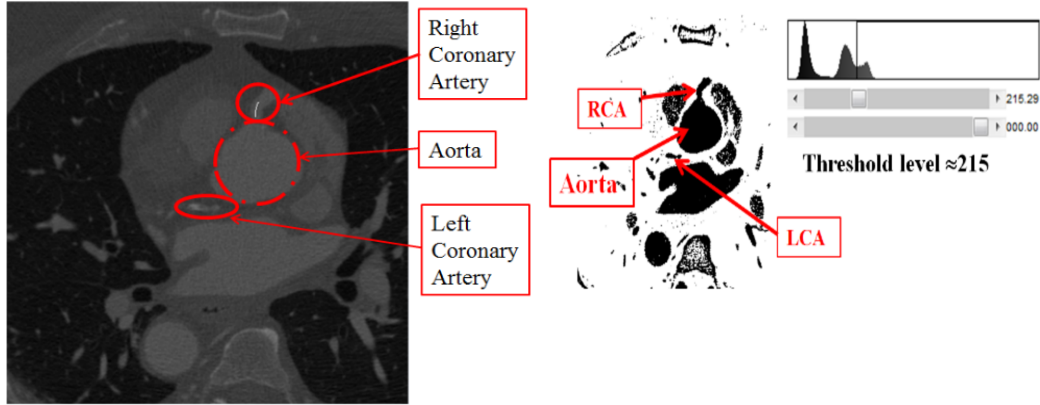
Fig. 7. Real patient data of cardiac CT slice represents the aorta, the right coronary artery (RCA), the left coronary artery (LCA). The thresholding based segmentation procedure.
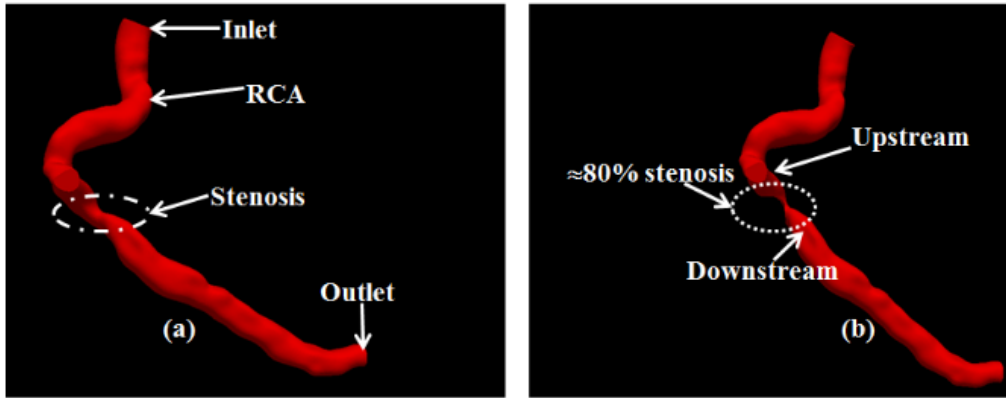

Fig. 8. The three-dimensional patient-specific (a) normal and (b) manually stenosed coronary artery models.

generation [25]. The algorithm provided a smooth surface reconstruction of 3D patient-specific model. Finally, the 3D model was ready for CFD simulation, but still some problems arose for CFD solver.

4.3 Mesh generation in 3D model

The mesh generation in CFD solver in the patient-based computational domain was a more difficult task because of the intersection of mesh components. For the robust mesh generation algorithm the marching cubes applied in 3D patient model. Due to the computational model complexity, it was not quite feasible to adapt 2D triangle and 3D tetrahedral meshing in the patient-specific model which already used in the 3D idealized model. A shrink wrapping approach was employed for remeshing in the computational complex domain [26]. The shrink wrapping algorithm converted the unstructured triangle mesh into subdivision connectivity. The idea of the shrink wrapping
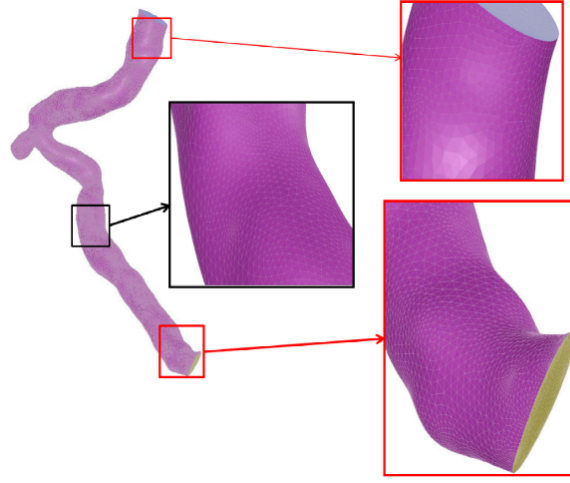
Fig. 9. Computational mesh generation in 3D patient-specific model and focus on the various segments of the patient-specific model.

technique is that the resulting algorithm generates subdivision connectivity meshes with a very small number of triangles for the deformable surfaces. For performing shrink wrapping mesh, at first, we imported .stl model file in the CFD solver. A bounding box was created over the model for the identification of inlet and the outlet. Then the materials for blood zone, surface zone and scope sizing for wrapping mesh were employed. For improving the quality mesh, the cells connectivity was an important tool and assigned small size with prism layers in the wall of the 3D model. Fig. 9 represents the tetrahedral shrink wrapping mesh with different segments. At last, the shrink wrapping mesh was ready and exported the 3D patient model for final CFD simulation.

4.4   Arterial input function and numerical simulation

In the patient-specific model, followed the same AIF in equation (3.1) for generating contrast agent concentration $C(t)$. The AIF produced the contrast agent concentration at the ostium of the coronary artery which employed for tracking the bolus at the reference position of CT scans. Fig.4 shows that the bolus tracking started at 50 HU after 10 seconds and the maximum enhancement of the contrast agent at 350 HU after 25 seconds. The contrast agent concentration revealed the blood flow of the 3D patient-specific coronary artery model which executed in the different stages that already discussed in the 3D idealized model. The fine mesh was generated in the patient-based model with the number of grid elements 456798. The same physical materials assigned in patient model, for instance, Reynolds number, blood density, pressure at the outlets which were assigned the same mechanisms in the ideal model. The computational results provided the relative pressure difference and velocity magnitude for the patient-specific model. In this case, the numerical simulation performed for the normal model and manually created about 80% stenosis model (Fig. 8). In unstenosed model, it was realized that there was a constriction region at the bending area in real patient's model. It was quite clear that, the simulation produced higher velocity magnitude in that narrow region than other locations. The pressure difference also quite distinguishable at the upstream and downstream difference of the constricted region. The CFD solver employed for solving the steady and pulsatile flow conditions. In steady case, the velocity magnitude of the stenosis area higher than the other region of the patient model and the value of the stenosis region

about 45 cm/s which were more than two times of the upstream velocity about 20 cm/s. In the pressure difference of stenosis model, we observed that the relative pressures in the upstream area were around 3.8 $mmHg$ and the downstream region approximately 2.5 $mmHg$ of the stenosis. The vFFR value was 0.65, which reflected that the stenosis was very significant. These properties of the CHD simulation results showed the physiological phenomena in the patient-specific model as expected.

## 4.5   Visualization of simulation results in patient models

The three hemodynamic parameters for the postprocessing of the simulation results were observed in the patient-specific model. The parameters such as the pressure difference, velocity magnitude and volume rendering for velocity magnitude were gave the functional information about the severity of coronary stenosis. Especially, the volume rendering provided the precise visualization of the blood flow velocity inside the 3D coronary arterial model. Fig. 10 has two rows, where the first row represents the velocity magnitude and the second row is the pressure difference in the steady blood flow condition.
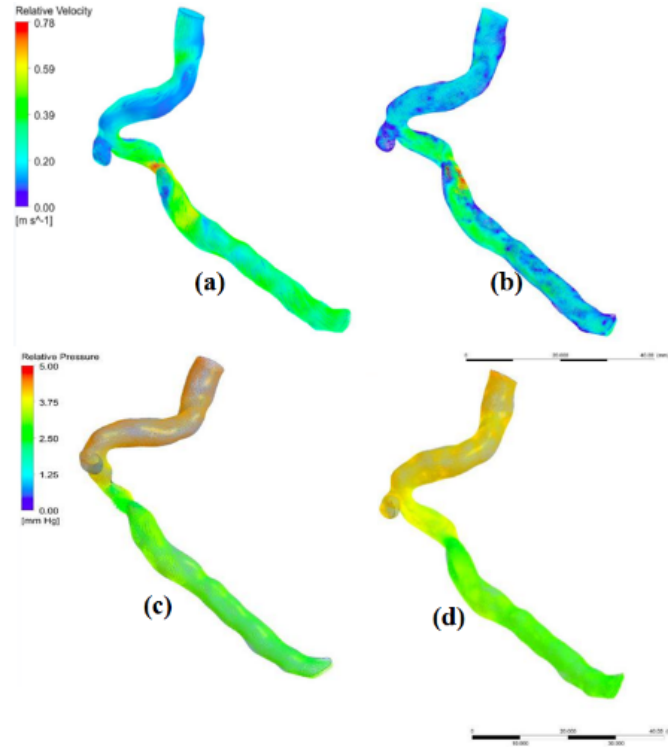
Fig. 10. Patient-based computational results of velocity magnitude and relative pressure visualization in normal patient model (a), (c) and stenosed model (b), (d) in steady flow.

The same scale and image orientation applied in both cases (normal and diseased) for velocity magnitude and relative pressure in the numerical simulation of the patient-based models. In Fig.10 **(a)** and **(c)**, the figures represent the computational simulation results of the unstenosed model and **(b)** and **(d)** are display the results of diseased model. The volume rendering images in Fig. 11

of the velocity magnitude images guaranteed about the stenosis condition. For the relative pressure difference, the **(c)** and **(d)** images (in Fig. 10 show the disease and healthy simulation results respectively. Fig.11 describes the volume rendering images in the **(a)** stenosis and **(b)** unstenosed
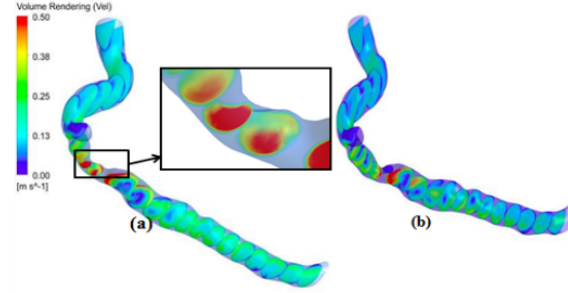
Fig. 11. Volume rendering of the velocity magnitude slices aligned in an outline of the coronary artery illustrating the stenosed area in steady flow simulations.

cases. Here attached an image segment of the stenosis region of the coronary artery blood flow velocity. The segmented image was allowed to identify the stenosis condition of the patient-specific model.
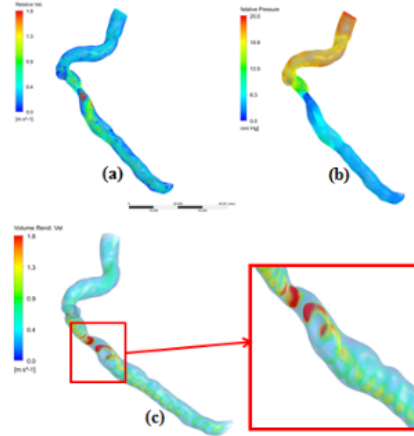
Fig. 12. Patient-based computational results of velocity magnitude, relative pressure and volume rendering of velocity magnitude with segmented part of the constriction region display in pulsatile flow state.

The same strategies assigned for pulsatile flow simulation with pulsatile function that discussed in the equation (2.3). The sinusoidal pressure difference equation (2.3) was similar with the periodic oscillation of the blood pulsatile flow nature. Due to the narrow region in the real patient's model, the numerical simulation was also quite distinct and produced higher velocity in the constricted region.

The Fig.12 representes the pulsatile flow simulation results of velocity magnitude, pressure difference and volume rendering of velocity magnitude in the patient-specific model. These characteristics reflected the physiological behavior of the real blood flow of the patient-specific numerical simulation.

5 Conclusion

The aim of the work was to set up a framework for an idealized and a patient-specific model reconstruction, geometric analysis and describing hemodynamic parameters.The parameters allowed to describe the intrinsic blood flow in a non-invasive procedure. This technique could be used as a complement procedure of the expensive and risky invasive catheterization test. This has been accomplished with the development of a set of techniques which provided the coronary severity information from coronary CTA data. The simulation results produced detailed information of the hemodynamic mechanisms that were compared with the experimental data. The results reflect expected outcomes in both cases, for instance, a higher blood velocity in the coronary vessels tends to stretch the contrast agent gradient and a lower blood velocity magnitude tends to steepen the contrast agent gradient. The pressure difference and vFFR results allowed to distinguish the unstenosed and stenosis arterial models. The simulation results are feasible for clinical applications but there are some limitations in the approaches which need more studies to overcome them.

Acknowledgement

Competing Interests

Authors have declared that no competing interests exist.

References

[1] Nichols M, et al. Cardiovascular disease in Europe 2014: Epidemiological update. European Heart Journal. 2014;35(42):2950-2959.

[2] Zamir M. Hemodynamics. Biological and medical physics, biomedical engineering. Springer International Publishing Switzerland; 2016.

[3] Taylor CA, et al. Computational fluid dynamics applied to cardiac computed tomography for noninvasive quantification of fractional flow reserve. J. of the Am. College of Cardiology. 2013; 61(22).
Available: http://dx.doi.org/10.1016/j.jacc.2012.11.083

[4] Westerhof N. Snapshots of hemodynamics: An aid for clinical research and graduate education. Springer (Florida). 2010;192.

[5] Park J, et al. Computational fluid dynamic measures of wall shear stress are related to coronary lesion characteristics. J. of Heart. 2016;1-8.

[6] Sun Z. Cardiac imaging modalities in the diagnosis of coronary artery diseases. J. Clin. Exp. Cardiology. 2013;S6.

[7] Zhang JM, et al. Simplified models of non-invasive fraction flow reserve based on ct images. PloS one 11, e0153070; 2016

[8] Malota Z, et al. Numerical analysis of the impact of flow rate, heart rate, vessel geometry and degree of stenosis on coronary hemodynamic indices. BMC Cardiovascular Disorders. 2018; 18(132):1-16.
Available: https://doi.org/10.1186/s12872-018-0865-6.

[9] Tu J, et al. Computational hemodynamics - Theory modelling and applications. Springer Science+Business Media Dordrecht; 2015.

[10] Bahrami S, Norouzi M. A numerical study on hemodynamics in the left coronary bifurcation with normal and hypertension condition. Biomechanics and Modeling in Mechanobiology. 2018;17:1-12.
Available: DOI: 10.1007/s10237-018-1056-1.

[11] Halpern EJ. Clinical application of cardiac CT angiography. J. of Insight Imaging (Springer). 2010;1:205-222.

[12] Kachelriess M. Iterative reconstruction techniques: What do they mean for cardiac ct ? curr. Cardiovasc Imaging Report. 2013;6:268-281.

[13] Papafaklis MI, et al. Functional assessment of lesion severity without using the pressure wire: Coronary imaging and blood flow simulation. Expert Review of Cardiovascular Therapy; 2017.
Available: http://dx.doi.org/10.1080/14779072.2017.1379899.

[14] Morris PD, et al. Fast virtual fractional flow reserve based upon steady-state computational fluid dynamics analysis. JACC: Basic to Translational Science. 2017;2(4):434-446.
Available: http://dx.doi.org/10.1016/j.jacbts.2017.04.003.

[15] Sun Z, Chaichana T. Computational fluid dynamic analysis of calcified coronary plaques: Correlation between hemodynamic changes and cardiac image analysis based on left coronary bifurcation angle and lumen assessments. J. of Interventional Cardiology. 2016;8(6):713-719.

[16] Zhong L, et al. Application of patient-specific computational fluid dynamics in coronary and intra-cardiac flow simulations: Challenges and opportunities. Front. Physiol. 2018; 9(742):1-17.
Available: DOI: 10.3389/fphys.2018.00742.

[17] Kays WM, Crawford ME. Convective heat and mass transfer, 3rd edition. McGraw-Hill. New York; 1993

[18] Dodge JT, et al. Lumen diameter of normal human coronary arteries. J. of Circulation. 1992;86(1):232-246.

[19] Spiegel M, et al. Tetrahedral vs. polyhedral mesh size evaluation on flow velocity and wall shear stress for cerebral hemodynamic simulation. J. of Comp. Methods Biomech. Biomed. Engineering. 2010;14:9-22.

[20] George RT, et al. A method for reconstructing the arterial input function during helical ct: Implications for myocardial perfusion distribution imaging. J. of Radiology. 2010;255(2):396-404.

[21] Eslami P, et al. Comutational study of computed tomography contrast gradients in models of stenosed coronary arteries. J. of Biomechanical Engineering. 2015;137(9):1-11.

[22] Chen X, et al. A clinical study on coronary artery blood velocity measured by digital tracing coronary angiography. J. of Pub. Medicine. 2007;24(2):294-298.

[23] Bruyne BD, et al. Fractional flow reserve-guided pci versus medical therapy in stable coronary disease. The New England Journal of Medicine. 2012;367(11):991-1001.

[24] Stein PD, et al. Sixty-four-slice ct for diagnosis of coronary artery disease: A systematic review. Am. J. of Medicine. 2008;121(8):715-725.

[25] Lorensen EL, Harvey EC. Marching cubes: A high resolution 3d surface construction algorithm. J. of Computer Graphics. 1987;21(4).

[26] Kobbelt, LP, et al. A Shrink wrapping approach to remeshing polygonal surfaces. J. of Eurographics. 1999;18(3).

Appendix

The 3D idealized model was generated by using FreeCAD, an open source software. FreeCAD allowed for curving the coronary ideal vessels, connecting the branches and creating the artificial stenosis manually. The CFD simulation conducted by two software, COMSOL Multiphysics 5.1 for idealized model and ANSYS Fluent student version 16.2 for patient-based model numerical simulation. We followed imagej open source software for the CT image segmentation and 3D reconstruction.

───